Superconductivity in $(NH_3)_yNa_xFeSe_{0.5}Te_{0.5}$

Lu Zheng, Yusuke Sakai, Xiao Miao, Saki Nishiyama, Takahiro Terao, Ritsuko Eguchi, Hidenori Goto, and Yoshihiro Kubozono*

Research Institute for Interdisciplinary Science, Okayama University, Okayama 700-8530, Japan

(Received 6 July 2016; revised manuscript received 29 September 2016; published 14 November 2016)

Na-intercalated $FeSe_{0.5}Te_{0.5}$ was prepared using the liquid NH_3 technique, and a superconducting phase exhibiting a superconducting transition temperature (T_c) as high as 27 K was discovered. This can be called the high-T_c phase since a 21 K superconducting phase was previously obtained in $(NH_3)_yNa_xFeSe_{0.5}Te_{0.5}$. The chemical composition of the high-T_c phase was determined to be $(NH_3)_{0.61(4)}Na_{0.63(5)}Fe_{0.85}Se_{0.55(3)}Te_{0.44(2)}$. The x-ray diffraction patterns of both phases show that a larger lattice constant c (i.e., $FeSe_{0.5}Te_{0.5}$ plane spacing) produces a higher T_c. This behavior is the same as that of metal-doped FeSe, suggesting that improved Fermi-surface nesting produces the higher T_c. The high-T_c phase converted to the low-T_c phase within several days, indicating that it is a metastable phase. The temperature dependence of resistance for both phases was recorded at different magnetic fields, and the critical fields were determined for both phases. Finally, the T_c versus c phase diagram was prepared for the metal-doped $FeSe_{0.5}Te_{0.5}$, which is similar to that of metal-doped FeSe, although the T_c is lower.

DOI: 10.1103/PhysRevB.94.174505

A number of superconductors have been synthesized by doping FeSe solids with metal atoms, establishing that this is a very effective way to realize alternative superconductors [1–15]. The metal doping has been achieved using a high-temperature annealing technique [1–6], a liquid solution technique [7–14], and an electrochemical technique [15]. However, the metal doping of $FeSe_{1-z}Te_z (z \neq 0)$ has only been reported in a few studies, in which doping was performed using the annealing and liquid solution techniques [16–18].

Solid FeSe showed a T_c as high as 8 K [19,20], while the T_c value of $FeSe_{1-z}Te_z$ made a domelike curve when plotted against z. The maximum T_c was 14 K for $z = 0.5$ in $FeSe_{1-z}Te_z$ [21]. Bulk FeTe crystals did not display superconductivity. This phase diagram attracted much attention because of the expectation that a high-T_c phase would be produced by the metal doping of $FeSe_{0.5}Te_{0.5}$. Sakai *et al.* doped $FeSe_{0.5}Te_{0.5}$ with various metal atoms using the liquid NH_3 technique [16], which provided T_c's of 17 K for $(NH_3)_yCa_{0.4}FeSe_{0.5}Te_{0.5}$, 21 K for $(NH_3)_yNa_{0.4}FeSe_{0.5}Te_{0.5}$, and 26 K for $(NH_3)_yLi_{0.4}FeSe_{0.5}Te_{0.5}$. Lei *et al.* investigated the z dependence of T_c in $(NH_3)_yM_xFeSe_{1-z}Te_z$ ($0 \leqslant z \leqslant 0.8$, M: Li and Na), and a T_c of 21 K was observed for $(NH_3)_yNa_xFeSe_{0.5}Te_{0.5}$ [18]. They determined the NH_3 quantity (y) to be 0.3–0.8 using liquid chromatography.

Recently, we discovered multiple superconducting phases in $(NH_3)_yNa_xFeSe$ [13], indicating that the Na atom occupies the on-center position (2*a* site) in the *I*4/*mmm* structure (on-center structure) when the x value is small, while the Na atom occupies the off-center position (2*b* site) in the *I*4/*mmm* lattice (off-center structure) when the x value is large. The lattice constant (c), is larger in the off-center structure, which provided the high-T_c phase.

In this study we discovered a superconducting phase of $(NH_3)_yNa_xFeSe_{0.5}Te_{0.5}$ with a T_c as high as 27 K. There are at least two superconducting phases of $(NH_3)_yNa_xFeSe_{0.5}Te_{0.5}$, with T_c values as high as 21 and 27 K, a property shared with $(NH_3)_yNa_xFeSe$. The x dependence of T_c was investigated in $(NH_3)_yNa_xFeSe_{0.5}Te_{0.5}$, as well as the physical properties and crystal structure of the high-T_c phase of $(NH_3)_yNa_xFeSe_{0.5}Te_{0.5}$. The stability of the just-discovered high-T_c phase was also checked. The temperature (T) dependence of resistance (R) was recorded for both phases ($T_c = 21$ K and $T_c = 27$ K) of $(NH_3)_yNa_xFeSe_{0.5}Te_{0.5}$, and the critical magnetic fields (H_c) of both phases were determined from their R versus T plots. Based on the T_c and c values of $(NH_3)_yNa_xFeSe_{0.5}Te_{0.5}$, the T_c versus c phase diagram was obtained, which was similar to that of metal-doped FeSe.

The β-$FeSe_{0.5}Te_{0.5}$ sample was prepared using the same method as that described in Ref. [16]. The samples of $(NH_3)_yNa_xFeSe_{0.5}Te_{0.5}$ were prepared using the liquid NH_3 technique [16]; the detailed experimental procedure was described in our previous report [16]. The magnetic susceptibility, M/H, of the samples was measured using a SQUID magnetometer (Quantum Design MPMS2); M and H refer to magnetization and applied magnetic field, respectively. The T_c and shielding fraction were 14.0 K and 100% at 2 K, respectively, for $FeSe_{0.5}Te_{0.5}$ (not shown).

The R of the samples was recorded in standard four-terminal measurement mode with a He cryostat regulated by a temperature controller (Oxford Instruments ITC503); the H was applied using an Oxford superconducting magnet system with variable temperature insert; the electric current (I) was supplied by a Keithley 220 programmable current source, and the voltage was measured by a Keithley Nanovoltmeter 2182. Four conducting wires for the R measurement were attached to each pellet of the high-T_c and low-T_c phase of $(NH_3)_yNa_xFeSe_{0.5}Te_{0.5}$ using silver paste (see Fig. S1 in the Supplemental Material [22]); the pellet was prepared at room temperature. The x-ray powder diffraction (XRD) patterns of the samples were measured with a Rigaku R-Axis Rapid-NR x-ray diffractometer with Mo $K\alpha$ source (wavelength $\lambda =$ 0.710 78 Å). The chemical composition of each sample was

*Corresponding author: kubozono@cc.okayama-u.ac.jp

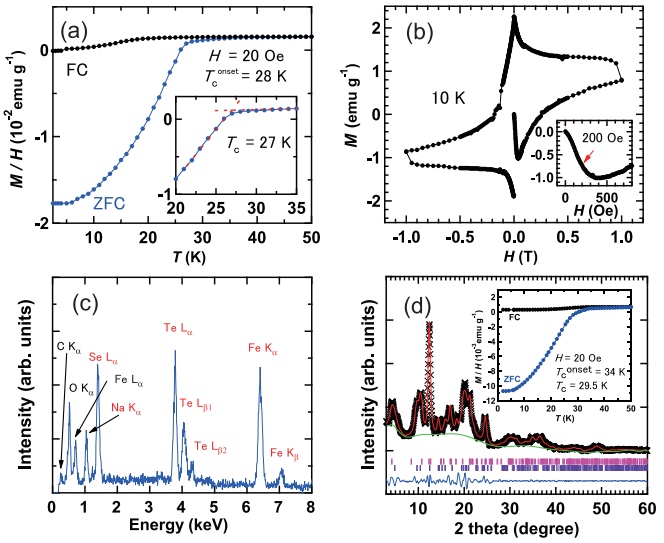

FIG. 1. Plots of (a) M/H versus T, (b) M versus H, and (c) EDX spectrum of the high-T_c phase of $(NH_3)_yNa_{0.4}FeSe_{0.5}Te_{0.5}$. (d) XRD pattern of the high-T_c phase of $(NH_3)_yNa_{0.6}FeSe_{0.5}Te_{0.5}$. In (a), the M/H versus T plots were recorded in ZFC and FC modes, and in the inset of (a), the method of defining T_c is shown; in the inset of (b), the expanded M versus H plot is shown, and the H_{c1} is obtained. In (c), an EDX peak is assigned to each element, and the red and black characters refer, respectively, to the elements used for the evaluation of chemical composition and those not thus used. In (d), the × (black) and solid (red) curves refer to the experimental XRD and the calculated pattern obtained by Le Bail fitting, respectively. The ticks (pink and purple) refer to the positions of the high-T_c and low-T_c phases, respectively. The green and blue curves refer to the background and the difference between the experimental and calculated XRD patterns, respectively.

determined by energy dispersive x-ray (EDX) spectroscopy with an EDX spectrometer equipped with a scanning electron microscope (SEM) (Keyence VE-9800–EDAX Genesis XM_2). Throughout this paper, the stoichiometric compositions of the samples prepared are expressed as the experimental nominal values, and the stoichiometric compositions of only two samples were experimentally determined. In this paper, the chemical formula of the samples described without additional comment refers to the experimental nominal values.

The M/H versus T plots of $(NH_3)_yNa_{0.4}FeSe_{0.5}Te_{0.5}$ are shown in Fig. 1(a). The T_c^{onset} and T_c values were determined to be 28 and 27 K, respectively. The shielding fraction was 84% at 10 K. The y value of this sample was found to be 0.61(4) from the mass difference before and after reaction with liquid NH_3. The T_c(=27 K) of this phase differed from that ($T_c = 21$ K) of the low-T_c phase of $(NH_3)_yNa_xFeSe_{0.5}Te_{0.5}$, which was previously reported [16,17]. Furthermore, the y value (=0.6–0.7) was quite different from the $y = 0.03(1)$ of the low-T_c phase [17]. In the low-T_c phase, a significant amount of NH_3 may not be included.

The M versus H plot of the high-T_c phase [$(NH_3)_yNa_{0.4}FeSe_{0.5}Te_{0.5}$] measured at 5 K is shown in Fig. 1(b); the sample used was the same as that used for Fig. 1(a). A diamond-shaped M versus H curve was clearly observed, showing superconductivity. The lower critical field, H_{c1}, was determined to be 200 Oe from the expanded M versus H plot shown in the inset of Fig. 1(b), which is higher than that (100 Oe) of the low-T_c phase [16]. Here, it should be noticed that the M plotted in Fig. 1(b) is smaller by a factor of 5 than that predicted from the M/H-T plot shown in Fig. 1(a). We do not know why the M becomes smaller than that predicted from Fig. 1(a). After the measurement of the M-H curve [Fig. 1(b)], the M/H-T plot was recorded again, which showed the same M/H-T plot as that shown in Fig. 1(a), indicating no sample degradation. Anyway, as the M-H curve suggests a linear variation of M against H up to 200 Oe, we concluded that 200 Oe is a reasonable value for H_{c1} in the high-T_c phase.

Figure 1(c) shows the EDX spectrum of the high-T_c phase of $(NH_3)_yNa_{0.4}FeSe_{0.5}Te_{0.5}$; the same sample was used for Figs. 1(a) and 1(b). The stoichiometric composition of the $(NH_3)_yNa_{0.4}FeSe_{0.5}Te_{0.5}$ sample was experimentally determined to be $(NH_3)_yNa_{0.63(5)}Fe_{0.85}Se_{0.55(3)}Te_{0.44(2)}$, in which $y = 0.61(4)$, i.e., $(NH_3)_{0.61(4)}Na_{0.63(5)}Fe_{0.85}Se_{0.55(3)}Te_{0.44(2)}$, where the Fe count was expressed as 0.85 so that the sum of Se and Te would be equal to 1.0. We confirmed that the y value fell within the range 0.6–0.7, using three different samples (high-T_c phase).

The XRD pattern of $(NH_3)_yNa_{0.6}FeSe_{0.5}Te_{0.5}$ is shown in Fig. 1(d); the sample was not that used for Figs. 1(a)–1(c), but its T_c was 30 K and the shielding fraction was 89% at 2 K; i.e., it was the high-T_c phase. The XRD pattern was analyzed by Le Bail fitting considering two phases, the high-T_c phase and low-T_c phase, the major phase being the high-T_c phase. The space group was $I4/mmm$ for both phases. The lattice constants a and c for the high-T_c phase were determined to be 3.874(2) and 19.33(1) Å, respectively. A trace of low-T_c phase was observed in the XRD pattern, and a and c were 4.029(2) and 16.84(1) Å, respectively. However, the c value was significantly different from the c[=17.798(7) Å] of the low-T_c phase reported previously [16], indicating that the exact c value could not be determined because so little of the low-T_c phase was contained in the sample. The a of the low-T_c phase reported previously was 3.9822(6) Å. Reliable values of a and c for the low-T_c phase are described later.

The high-T_c and low-T_c phases of $(NH_3)_yNa_xFeSe$ were selectively prepared by varying the concentration of intercalated Na atoms, i.e., the x value [13]. The high-T_c phase in $(NH_3)_yNa_xFeSe$ was obtained with high x values, while the low-T_c phase was produced in samples with low x values. Figure 2(a) shows the T_c values of the $(NH_3)_yNa_xFeSe_{0.5}Te_{0.5}$ samples prepared with various experimental nominal x values. Two clearly distinguished T_c values ($T_c = 28$ K and $T_c = 21$ K) were recorded for the $(NH_3)_yNa_xFeSe_{0.5}Te_{0.5}$ samples, although some scattering around the above values was observed. However, no clear correlation between T_c and x was found from the T_c versus x plot shown in Fig. 2(a). Here, it should be noticed that the x corresponds to the experimental nominal value. Therefore, we may need to consider the difference between nominal and actual x values for understanding why there is no clear correlation [Fig. 2(a)]. From the plot shown in Fig. 2(a), only a presence of two different T_c's was clearly found in $(NH_3)_yNa_x$ $FeSe_{0.5}Te_{0.5}$.

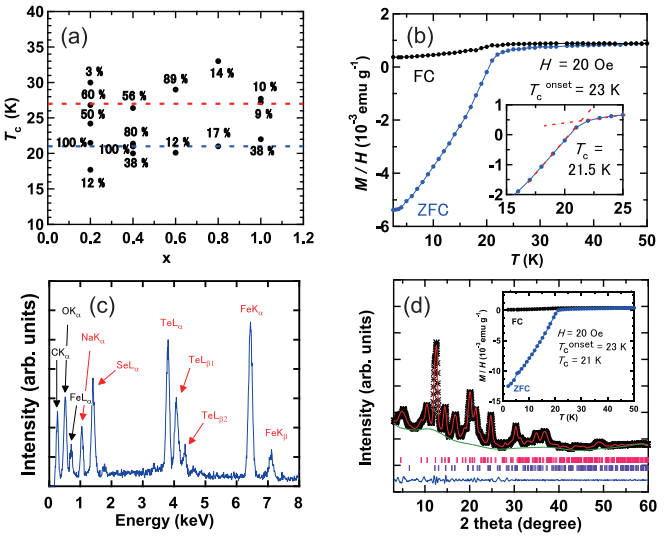

FIG. 2. (a) Plots of T_c against experimental nominal values of x in $(NH_3)_yNa_xFeSe_{0.5}Te_{0.5}$. The T_c was plotted for 16 samples prepared in this study. (b) Plots of M/H versus T, (c) EDX spectrum, and (d) XRD pattern of the low-T_c phase of $(NH_3)_yNa_{0.4}FeSe_{0.5}Te_{0.5}$. In (a), the shielding fractions at 2.5 K are shown. In (b) the M/H versus T plots were recorded in ZFC and FC modes. In the inset of (b), the method for defining T_c is shown; the M/H versus T plot was obtained in ZFC mode. In (c), the EDX peak is assigned to each element, and the red and black characters, respectively, refer to the elements used for the evaluation of chemical composition and those not so used. In (d), the × (black) and solid curves (red) refer to the experimental XRD and the calculated pattern obtained by Le Bail fitting, respectively. The ticks (pink and purple) refer to the positions of the low-T_c phase and pristine $FeSe_{0.5}Te_{0.5}$, respectively. The green and blue curves refer, respectively, to the background and the difference between the experimental and calculated XRD patterns.

Figure 2(b) shows the M/H versus T curves of the typical low-T_c phase of $(NH_3)_yNa_{0.4}FeSe_{0.5}Te_{0.5}$. The T_c^{onset} and T_c values were determined to be 23 and 21.5 K from the M/H versus T curve recorded in zero field cooled (ZFC) mode [Fig. 2(b)]. The shielding fraction was 28% at 10 K for this sample. Figure 2(c) shows the EDX spectrum of the low-T_c phase, indicating chemical stoichiometry of $(NH_3)_{0.03(1)}Na_{0.7(3)}Fe_{1.33}Se_{0.48(9)}Te_{0.52(5)}$; the value of Fe was set at 1.33 so that the sum of Se and Te would be 1.0, as was done for the high-T_c phase. The amount of NH_3 (y value) was determined to be 0.03(1) from the mass difference before and after reaction with liquid NH_3. Consequently, the amount of NH_3 is too small in the low-T_c phase.

The XRD pattern of the low-T_c phase, $(NH_3)_yNa_{0.4}FeSe_{0.5}Te_{0.5}$, is shown in Fig. 2(d). The XRD was analyzed by Le Bail fitting considering two phases, the low-T_c phase and pristine $FeSe_{0.5}Te_{0.5}$; the space group was $I4/mmm$ for the low-T_c phase and $P4/nmm$ for pristine $FeSe_{0.5}Te_{0.5}$. The major phase was the low-T_c phase, and the a and c were determined to be 3.9824(6) and 17.787(7) Å, respectively, which are consistent with the values $a = 3.9822(6)$ Å and $c = 17.798(7)$ Å reported previously for the low-T_c phase [16]. The c of the high-T_c phase is larger by 1.543 Å than that of the low-T_c phase, indicating that a larger

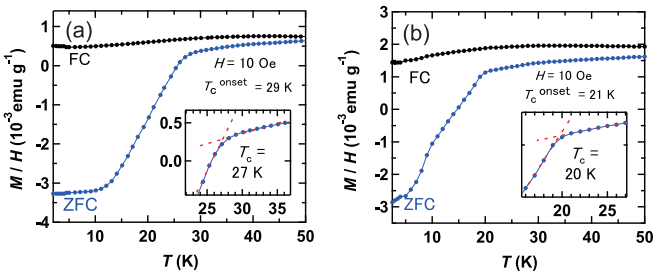

FIG. 3. Plots of M/H versus T of $(NH_3)_yNa_{0.5}FeSe_{0.5}Te_{0.5}$ measured (a) just after preparation and (b) after 3 days of preparation. In (a) and (b), the M/H versus T plots were recorded in ZFC and FC modes. In the insets of (a,b), the method for defining T_c is shown; the M/H versus T plots were obtained in ZFC mode.

c produces a higher T_c, as also observed in $(NH_3)M_xFeSe$ (M: alkali and alkali earth metal atoms) [9,12,13]. The space group is the same in the high-T_c and low-T_c phases, indicating that only the location of Na is different in each, as previouly discussed for $(NH_3)_yNa_xFeSe$ [13]; we previously suggested that the Na occupies the on-center position in the low-T_c phase and the off-center position in the high-T_c phase, under the space group of $I4/mmm$. Therefore, we substantially assume the same scenario for the high-T_c and low-T_c phases of $(NH_3)_yNa_xFeSe_{0.5}Te_{0.5}$. On the other hand, Sedlmaier *et al.* suggested the primitive tetragonal structure ($P4/n$ or $P4/nmm$) for NH_3-rich M_xFeSe (M: Li, K, and Rb), with more expanded FeSe plane spacing than that in the body-centered tetragonal structure ($I4/mmm$) [10]. At the present stage, we cannot conclude whether the high-T_c phase of $(NH_3)_yNa_xFeSe_{0.5}Te_{0.5}$ (NH_3-rich structure) takes such a primitive tetragonal structure. More detailed analysis using Rietveld refinement is necessary to determine the precise crystal structure.

The M/H versus T plot for $(NH_3)_yNa_{0.5}FeSe_{0.5}Te_{0.5}$ (T_c = 27 K and shielding fraction = 18% at 10 K) is shown in Fig. 3(a), and can be assigned to the high-T_c phase. However, the M/H versus T plot changed drastically after 3 days, as shown in Fig. 3(b). The T_c changed to 20 K from 27 K, implying conversion from the high-T_c to the low-T_c phase, indicating that the high-T_c phase is a metastable phase. Such a conversion was frequently observed in this study. Therefore, it is necessary to investigate the physical properties of the high-T_c phase quickly, before the conversion. No conversion was found on a scale of several days in $(NH_3)_yNa_xFeSe$, although no investigation of conversion was performed for longer time scales, such as a year.

The temperature dependence of R for the high-T_c and low-T_c phases at different H's is presented in Figs. 4(a) and 4(b), respectively. The T_c^{onset} and T_c values were determined to be 31 and 27 K, respectively, from the M/H versus T plot for the high-T_c phase [inset of Fig. 4(a)], while they were 23 and 21 K for the low-T_c phase [inset of Fig. 4(b)]. As seen from Figs. 4(a) and 4(b), zero R was not observed for either phase because of the use of pellets fabricated from polycrystalline powder samples. No observation of zero R is the same as that in Na- and Ba-doped FeSe prepared using liquid NH_3 [7]. As seen from Figs. 4(a) and 4(b), the T_c^{onset} and T_c decrease monotonically in both phases with

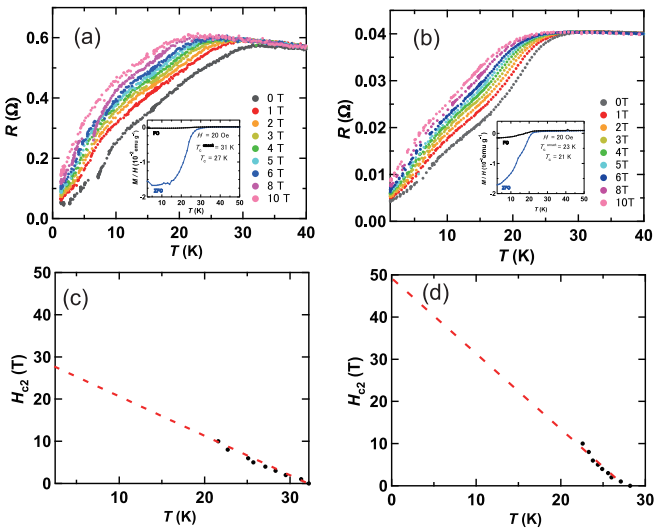

FIG. 4. Plots of R versus T for (a) high-T_c and (b) low-T_c phases of $(NH_3)_yNa_xFeSe_{0.5}Te_{0.5}$ at different H's. In the insets of (a,b), plots of M/H versus T are provided to show the superconductivity of the samples. The applied H's are shown by solid circles with different colors. Plots of H_{c2} versus T for (c) the high-T_c and (d) low-T_c phases determined from the R versus T plots recorded at different H's. The fitted lines are linear best fits.

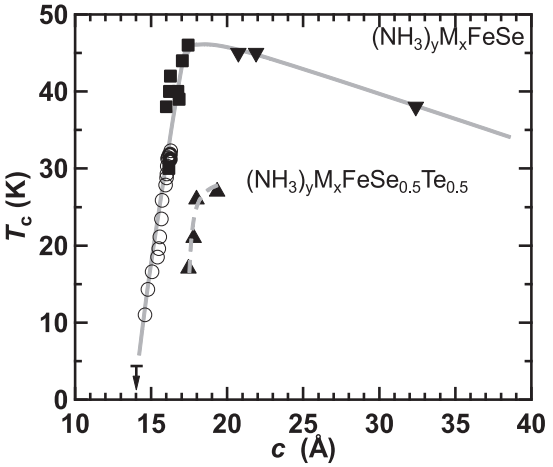

FIG. 5. Plots of T_c against c for $(NH_3)M_xFeSe$ and $(NH_3)_yM_xFeSe_{0.5}Te_{0.5}$. For the former, the eye guide is a solid line, for the latter, a dashed line. Solid squares and solid circles refer, respectively, to the T_c values against c for $(NH_3)M_xFeSe$ obtained from Refs. [7,9]. The solid inverse triangles refer to the T_c values against c in $(amine)_yM_xFeSe$ in which various amines were used in sample preparation; the data were obtained from Ref. [12]. The solid triangle plots refer to T_c values against $(NH_3)_yM_xFeSe_{0.5}Te_{0.5}$ (this paper and Ref. [16]). Open circles refer to the plots obtained from the pressure dependence of $(NH_3)_yCs_xFeSe$ in Ref. [24].

the application of increasing H. In other words, the onset of R drop shifts to a lower temperature, indicating that the R drop can be assigned to a superconducting transition. The H_{c2} values were evaluated from the T_c^{onset} at each H. The H_c versus T plots for the high-T_c and low-T_c phases are provided in Figs. 4(c) and 4(d). The H_{c2} values at 0 K [$H_{c2}(0)$] for the high-T_c and low-T_c phases were, respectively, evaluated to be 20 and 34 T with the Werthamer-Helfand-Hohenberg formula, $H_{c2}(0) = -0.693T_c\ (dH_{c2}/dT)_{T=T_c}$; the values of H_{c1} were 200 and 100 Oe for high-T_c and low-T_c phases, as described previously. London penetration depth (λ) and Ginzburg-Landau coherent length (ξ_{GL}) are determined to be 1.8×10^2 and 4.1 nm for the high-T_c phase, respectively, and 2.6×10^2 and 3.1 nm for the low-T_c phase, using the formulas $H_{c2} = \frac{\Phi_0}{2\pi\xi_{GL}^2}$, and $H_{c1} = \frac{\Phi_0}{4\pi\lambda^2}\ln(\frac{\lambda}{\xi_{GL}})$, where $\Phi_0(\approx 2.0678 \times 10^{-7}\,G\,cm^2)$ is a quantum magnetic flux [23]. The values of the Ginzburg-Landau parameter, κ, were more than $1/\sqrt{2}$ for both phases, indicating that these phases are categorized as "type-II superconductor."

Finally, the T_c was plotted as a function of c for $(NH_3)_yM_xFeSe$ and $(NH_3)_yM_xFeSe_{0.5}Te_{0.5}$ in Fig. 5, where M represents alkali and alkali earth metal atoms, the plots are based on data in this paper and previous articles on various metal-doped FeSe and $FeSe_{0.5}Te_{0.5}$ (Refs. [7,9,12]), and the pressure dependence of T_c in $(NH_3)_yCs_xFeSe$ [24]. Previously, we showed a clear correlation between T_c and c for $(NH_3)_yM_xFeSe$, and the saturation of T_c with more expanded FeSe plane spacing [9,12,13]. As seen from Fig. 5, the T_c versus c behavior for $(NH_3)_yM_xFeSe_{0.5}Te_{0.5}$ is similar to that of $(NH_3)_yM_xFeSe$, although the T_c of the former is lower than that of the latter. Namely, in $(NH_3)_yM_xFeSe_{0.5}Te_{0.5}$, the T_c increases with increasing c, as in $(NH_3)_yM_xFeSe$, in which it saturates or decreases at larger c. Here, we did not remark on the difference in carrier concentration between high-T_c and low-T_c phases, because no clear correlation between x and T_c was observed. Furthermore, we found only two superconducting phases even when changing x continuously in $(NH_3)_yNa_xFeSe_{0.5}Te_{0.5}$ and $(NH_3)_yNa_xFeSe$ [13], suggesting that a different T_c may not originate from the difference in carrier concentration. In other words, the T_c can be substantially scaled with the FeSe or $FeSe_{0.5}Te_{0.5}$ plane spacing. The increase in T_c against c can be simply explained by the improved Fermi-surface nesting allowed by the expanded FeSe or $FeSe_{0.5}Te_{0.5}$ layer spacing (or increase in two dimensionality), while the saturation and decrease in T_c for the more expanded layer spacing implies that the extremely small interaction between layers has a negative effect on superconductivity; i.e., interaction between layers is required for the emergence of superconductivity. These properties of metal-doped $FeSe_{1-z}Te_z$ superconductors may open an avenue for the realization of metal-doped Fe chalcogenide materials with higher T_c values.

The authors thank Professor Yoshihiro Iwasa of the University of Tokyo for kindly permitting us to use the XRD equipment in his laboratory. This study was partly supported by a grant-in-aid (Grants No. 22244045, No. 24654305, and No. 26105004) from Ministry of Education, Culture, Sports, Science, and Technology (MEXT), Japan, the LEMSUPER project (JST-EU Superconductor Project), the JST-ACTC project of the Japan Science and Technology Agency (JST), and the MEXT Program for Promoting the Enhancement of Research Universities. Furthermore, this study was supported by the JSPS Program for Advancing Strategic International Networks to Accelerate the Circulation of Talented Researchers.

[1] J. Guo, S. Jin, G. Wang, S. Wang, K. Zhu, T. Zhou, M. He, and X. Chen, Phys. Rev. B **82**, 180520(R) (2010).
[2] A. Krzton-Maziopa, Z. Shermadini, E. Pomjakushina, V. Pomjakushin, M. Bendele, A. Amato, R. Khasanov, H. Luetkens, and K. Conder, J. Phys.: Condens. Matter **23**, 052203 (2011).
[3] L. Sun, X.-J. Chen, J. Guo, P. Gao, Q.-Z. Huang, H. Wang, M. Fang, X. Chen, G. Chen, Q. Wu, C. Zhang, D. Gu, X. Dong, L. Wang, K. Yang, A. Li, X. Dai, H.-K. Mao, and Z. Zhao, Nature **483**, 67 (2012).
[4] A. Zhang, T.-L. Xia, K. Liu, W. Tong, Z.-R. Yang, and Q.-M. Zhang, Sci. Rep. **3**, 1216 (2013).
[5] Z. Shermadini, A. Krzton-Maziopa, M. Bendele, R. Khasanov, H. Luetkens, K. Conder, E. Pomjakushina, S. Weyeneth, V. Pomjakushin, O. Bossen, and A. Amato, Phys. Rev. Lett. **106**, 117602 (2011).
[6] X. Ding, D. L. Fang, Z. Y. Wang, H. Yang, J. Z. Liu, Q. Deng, G. B. Ma, C. Meng, Y. H. Hu, and H.-H. Wen, Nat. Commun. **4**, 1897 (2013).
[7] T. P. Ying, X. L. Chen, G. Wang, S. F. Jin, T. T. Zhou, X. F. Lai, H. Zhang, and W. Y. Wang, Sci. Rep. **2**, 426 (2012).
[8] M. Burrard-Lucas, D. G. Free, S. J. Sedlmaier, J. D. Wright, S. J. Cassidy, Y. Hara, A. J. Corkett, T. Lancaster, P. J. Baker, S. J. Blundell, and S. J. Clarke, Nat. Mater. **12**, 15 (2013).
[9] L. Zheng, M. Izumi, Y. Sakai, R. Eguchi, H. Goto, Y. Takabayashi, T. Kambe, T. Onji, S. Araki, T. C. Kobayashi, J. Kim, A. Fujiwara, and Y. Kubozono, Phys. Rev. B **88**, 094521 (2013).
[10] S. J. Sedlmaier, S. J. Cassidy, R. G. Morris, M. Drakopoulos, C. Reinhard, S. J. Moorhouse, D. O'Hare, P. Manuel, D. Khalyavin, and S. J. Clarke, J. Am. Chem. Soc. **136**, 630 (2014).
[11] T. Ying, X. Chen, G. Wang, S. Jin, X. Lai, T. Zhou, H. Zhang, S. Shen, and W. Wang, J. Am. Chem. Soc. **135**, 2951 (2013).
[12] T. Hatakeda, T. Noji, S. Hosono, T. Kawamata, M. Kato, and Y. Koike, J. Phys.: Conf. Ser. **568**, 022032 (2014).
[13] L. Zheng, X. Miao, Y. Sakai, M. Izumi, H. Goto, S. Nishiyama, E. Uesugi, Y. Kasahara, Y. Iwasa, and Y. Kubozono, Sci. Rep. **5**, 12774 (2015).
[14] L. Zheng, X. Miao, Y. Sakai, H. Goto, E. Uesugi, R. Eguchi, S. Nishiyama, K. Sugimoto, A. Fujiwara, and Y. Kubozono, Phys. Rev. B **93**, 104508 (2016).
[15] Y. Takahei, K. Tomita, Y. Itoh, K. Ashida, J.-H. Lee, N. Nishimoto, T. Kimura, K. Kudo, M. Nohara, Y. Kubozono, and T. Kambe, Sci. Rep. **6**, 18931 (2016).
[16] Y. Sakai, L. Zheng, M. Izumi, K. Teranishi, R. Eguchi, H. Goto, T. Onji, S. Araki, T. C. Kobayashi, and Y. Kubozono, Phys. Rev. B **89**, 144509 (2014).
[17] Y. Sakai, Study on superconductivity of metal-intercalated iron chalcogenides prepared using liquid ammonia technique, Master's thesis, Okayama University, 2015.
[18] H. Lei, J. Guo, F. Hayashi, and H. Hosono, Phys. Rev. B **90**, 214508 (2014).
[19] F.-C. Hsu, J.-Y. Luo, K.-W. Yeh, T.-K. Chen, T.-W. Huang, P. M. Wu, Y.-C. Lee, Y.-L. Huang, Y.-Y. Chu, D.-C. Yan, and M.-K. Wu, Proc. Natl. Acad. Sci. USA **105**, 14262 (2008).
[20] T. M. McQueen, Q. Huang, V. Ksenofontov, C. Felser, Q. Xu, H. Zandbergen, Y. S. Hor, J. Allred, A. J. Williams, D. Qu, J. Checkelsky, N. P. Ong, and R. J. Cava, Phys. Rev. B **79**, 014522 (2009).
[21] Y. Mizuguchi and Y. Takano, J. Phys. Soc. Jpn. **79**, 102001 (2010).
[22] See Supplemental Material at http://link.aps.org/supplemental/10.1103/PhysRevB.94.174505 for a photo of the $(NH_3)_yNa_xFeSe$ pellet used for four-terminal R measurement.
[23] M. Tinkham, *Introduction to Superconductivity* (McGraw-Hill, New York, 1975).
[24] M. Izumi, Lu. Zheng, Y. Sakai, H. Goto, M. Sakata, Y. Nakamoto, H. L. T. Nguyen, T. Kagayama, K. Shimizu, S. Araki, T. C. Kobayashi, T. Kambe, D. Gu, J. Guo, J. Liu, Y. Li, L. Sun, K. Prassides, and Y. Kubozono, Sci. Rep. **5**, 9477 (2015).